2D frequency-domain elastic full-waveform inversion using a P_0 finite volume forward problem

Romain Brossier [*], *Jean Virieux* [†] *and Stéphane Operto* [*] , [*] *Géosciences Azur - Université Nice Sophia-Antipolis* , [†] *Laboratoire de Géophysique Interne et Tectonophysique, Université Joseph Fourier*

SUMMARY

We present a 2-D frequency-domain elastic full-waveform inversion algorithm based on a forward problem solved with a frequency-domain parsimonious P_0 finite-volume method. A preconditioned conjugate gradient method allows the reconstruction of elastic parameters for various acquisition configurations. Solving many times the forward problem is required in the main steps of the inversion algorithm. In the frequency domain, the forward problem reduces to the resolution of a huge and sparse linear system which is efficiently performed with a massively parallel direct solver. The designed algorithm is validated with three simple synthetic examples for the reconstruction of both P and S wave velocities from vertical and horizontal particle velocities in regular equilateral triangular meshes.

INTRODUCTION

Quantitative seismic imaging of elastic parameters is one of the main challenge of geophysical exploration at different scales (subsurface, oil exploration, crustal and lithospheric investigations). Frequency-domain full-waveform inversion (FWI) (Pratt and Worthington, 1990; Pratt et al., 1996, 1998) allows to build accurate velocity models of complex structures from long offset acquisition geometries using only few discrete frequencies thanks to the wavenumber redundancy provided by multi-aperture geometries. Moreover, proceeding sequentially from the low frequencies to the high ones defines a multiresolution imaging strategy which helps to fulfill the assumptions underlying local optimization approaches. Applications to real data using the acoustic approximation for 2D geometries have been performed with success for imaging complex structures (Ravaut et al., 2004; Operto et al., 2006), while the reconstruction of elastic parameters has been found to be a quite challenging problem (Gelis et al., 2007) mainly due to the high numerical cost of the forward problem. Recently, a 2D parsimonious P_0 Finite Volume (FV) method has been proposed by Brossier et al. (2007) for accurate and efficient elastic wave modeling on triangular meshes. Accurate modeling of wave propagation for complicated topographies is achieved for a discretization of 15 triangular cells per minimum wavelength which leads to significant memory and CPU-time savings compared to that required by $O(\Delta x^2)$ Finite Difference (FD) methods. In this study, we present a massively parallel frequency-domain FWI algorithm for imaging 2D elastic parameters based on the P_0 FV forward problem and solved using a massively parallel direct solver. The algorithm is validated with three simple synthetic examples.

THEORY

Forward problem

The 2D elastic P-SV wave equation in the frequency domain is described by the following first order velocity-stress system:

$$\begin{aligned}
-\imath\omega V_x &= \frac{1}{\rho(\mathbf{x})}\Big\{\frac{\partial\sigma_{xx}}{\partial x}+\frac{\partial\sigma_{xz}}{\partial z}\Big\}+F_x \\
-\imath\omega V_z &= \frac{1}{\rho(\mathbf{x})}\Big\{\frac{\partial\sigma_{xz}}{\partial x}+\frac{\partial\sigma_{zz}}{\partial z}\Big\}+F_z \\
-\imath\omega\sigma_{xx} &= \big(\lambda(\mathbf{x})+2\mu(\mathbf{x})\big)\frac{\partial V_x}{\partial x}+\lambda(\mathbf{x})\frac{\partial V_z}{\partial z}-\imath\omega\sigma_{xx_0} \\
-\imath\omega\sigma_{zz} &= \lambda(\mathbf{x})\frac{\partial V_x}{\partial x}+\big(\lambda(\mathbf{x})+2\mu(\mathbf{x})\big)\frac{\partial V_z}{\partial z}-\imath\omega\sigma_{zz_0} \\
-\imath\omega\sigma_{xz} &= \mu(\mathbf{x})\Big\{\frac{\partial V_x}{\partial z}+\frac{\partial V_z}{\partial x}\Big\}-\imath\omega\sigma_{xz_0}, \qquad (1)
\end{aligned}$$

where (V_x,V_z) are the particles velocities, $(\sigma_{xx},\sigma_{zz},\sigma_{xz})$ the stresses, λ, μ are the Lamé coefficients, ρ the density and ω the angular frequency. External excitations are given by (F_x,F_z) for forces and $(\sigma_{xx_0},\sigma_{zz_0},\sigma_{xz_0})$ for stresses. Perfectly Matched Layers (Berenger, 1994) are introduced in system 1 as absorbing conditions to avoid parasite reflections from grid boundaries.
Medium is discretized with triangular cells and a parsimonious P_0 FV method is applied to system 1 (Brossier et al., 2007). Triangular description of medium allows to model accurately complex topographies without the staircase description commonly used in classical FD methods. We finally end up with a linear system which can be recast in a matrix form, with two particles velocities unknowns per triangular cell:

$$\mathbf{AV}=\mathbf{S} \qquad (2)$$

where the complex-value impedance matrix $\mathbf{A}$ depends on the frequency and the medium properties.
The P_0 FV approach leads to compact spatial stencil similar to that of $O(\Delta x^2)$ FD methods which limits the numerical bandwidth of the matrix and hence its fill-in during LU factorization compared to higher order ones (Hustedt et al., 2004). The P_0 FV approach requires 10 cells per minimum shear wavelength to obtain acceptable dispersion properties when horizontal free surface is considered and 15 cells when complex topographies are considered for propagation distances lower than 100 wavelengths. Due to the low order of P_0 interpolation, only regular equilateral meshes provide solutions with an acceptable accuracy. Unstructured meshes do not provide enough accurate solutions for FWI applications.
The LU factorization, although memory demanding, allows to solve efficiently thousands of forward problems since the factorization is independent of the right-hand side source terms in the equation 2. In this study, we used the massively parallel direct solver MUMPS which has been developed for distributed-memory platform (Amestoy et al., 2006).

Frequency-domain full-waveform inversion

The inverse problem is solved with a standard weighted least-squares preconditioned conjugate gradient method (Tarantola, 1987) for elastic parameters reconstruction. The Born approxi-

mation is used for computing the gradient of the objective function while the full solution of the forward problem is recomputed at each iteration of the inverse problem using the FV method in a way similar to the FD method proposed by Gelis et al. (2007). The weighted least-squares objective function is given by

$$\mathscr{C}(\mathbf{m}) = \Delta\mathbf{d}^{\dagger}\mathbf{W}_d\Delta\mathbf{d} \tag{3}$$

where $\Delta\mathbf{d}$ is the residuals for horizontal and vertical particle velocities (the difference between the observed data and the data computed with model $\mathbf{m}$), the superscript † indicates the adjoint (transpose conjugate) and $\mathbf{W}_d$ is a weighting operator applied to the data. Minimization of the cost function leads to the following solution for the model perturbation $\Delta\mathbf{m}$ after preconditioning the gradient (Pratt et al., 1998; Operto et al., 2006).

$$\Delta m_i = -\alpha(\hat{\mathbf{H}}_a + \varepsilon I)^{-1}\mathbf{S}\mathscr{G}_{\mathbf{m}} \tag{4}$$

where $\mathscr{G}_{\mathbf{m}}$ is the gradient of the objective function defined by

$$\mathscr{G}_{\mathbf{m}} = \mathscr{R}\left\{\mathbf{V}^t[\frac{\partial\mathbf{A}^t}{\partial m_i}]\mathbf{A}^{-1}\mathbf{W}_d\Delta\mathbf{d}^*\right\} \tag{5}$$

and $\hat{\mathbf{H}}_a = diag\mathscr{R}\{\mathbf{J}^t\mathbf{W}_d\mathbf{J}^*\}$ denotes the diagonal elements of the weighted approximate Hessian $\mathbf{H_a}$ and $\mathbf{J}$ denotes the sensitivity matrix. The detailed expression of the gradient of the objective function as a function of the elastic Green functions is provided in Gelis et al. (2007). One element of the sensitivity matrix is given by

$$\mathbf{J}_{k(m,n),i} = \mathbf{V}_m^t\left[\frac{\partial\mathbf{A}^t}{\partial m_i}\right]\mathbf{A}^{-1}\delta_n. \tag{6}$$

where $k(m,n)$ denotes a source/receiver-component couple of the acquisition system, m and n denotes one shot and one receiver component respectively. δ_n is a source vector describing one impulsional source in the direction of the receiver component n.

The diagonal of the approximate Hessian $\hat{\mathbf{H}}_a$ provides a preconditioner of the gradient which properly scales the perturbation model (Shin et al., 2001). The damping parameter ε is used to avoid numerical instabilities (i.e. division by zero). The matrix $\mathbf{S}$ is a smoothing regularization operator implemented in the form of a 2D Gaussian spatial filter (Ravaut et al., 2004). The term $\partial\mathbf{A}/\partial\mathbf{m_i}$ is the radiation pattern of the diffraction by the model parameter m_i (Tarantola, 1986). The parameter α is the descent steplength computed by a parabola fitting along the descent direction. The linearized inversion procedure is applied in cascade to several frequencies (or groups of discrete frequencies). For each frequency group, several iterations are computed. The use of conjugate directions of the gradient with Polak-Ribierre method (Mora, 1987) allows to speed up convergency of our algorithm.

Parallel Implementation

Two central ingredients of the FWI algorithm is the computation of the gradient $\mathscr{G}_{\mathbf{m}}$ and its preconditioner $\hat{\mathbf{H}}_a$. These two operators are basically computed by a weighted product of the forward problem solutions, namely the incident wavefields and the backpropagated residual wavefields computed in the starting model (equations 5 & 6). In order to compute in parallel $\mathscr{G}_{\mathbf{m}}$ and $\hat{\mathbf{H}}_a$, we take advantage of the distributed storage of the LU decomposition provided by the MUMPS solver: each processor stores a subdomain of LU factors of impedance matrix $\mathbf{A}$ and all the corresponding partial solutions. Therefore, each processor computes a part of the gradient and of the preconditioner according to the domain decomposition of the distributed forward problem. Due to the non-diagonal pattern of derivative matrix $\partial\mathbf{A}/\partial\mathbf{m_i}$, point-to-point communications are required between processors to exchange solutions for all cells located at interfaces between subdomains. Figure 1 summarized the parallel FWI algorithm.

VALIDATION TESTS

In this section, we validate our algorithm with three simple numerical examples. The two first examples use only body waves (i.e. absorbing conditions are applied on the four edges of model) to image an elastic layer embedded in a homogeneous background from a multichannel seismic reflection acquisition and small P- and S-wave velocity (hereinafter referred to as V_P and V_S) anomalies from a crosshole geometry respectively. Aim of the third example is to reconstruct a V_P and V_S anomalies in a velocity gradient model below a Gaussian topography. All these examples were performed in regular equilateral meshes to guarantee accurate propagation modeling.

Layer Model

The Layer model of dimension $8 \times 3.5\ km^2$ is composed of an homogeneous background with a 100-m thick horizontal layer. P-wave velocities are 3500 m/s and 3700 m/s in the background and in the layer respectively while the S-wave velocities are 2020 m/s and 2140 m/s respectively. Eighty vertical-force sources with a 80-m spacing are located 1300 m above the layer. The receiver array located 1400 m above the layer corresponds to 86 vertical and horizontal geophones with a 80-m spacing. Inversion for imaging V_P and V_S was sequentially applied to frequencies 1.96, 3.91, 5.87, 7.82, 9.8 and 12.7 Hz using the homogeneous background models as starting models. The frequency interval was chosen in order to preserve some wavenumber redundancy according to the Sirgue and Pratt (2004) rule. The gradient method without conjugate directions was used for this test. Ten iterations were computed per frequency. The correct V_P and V_S values were reconstructed in the layer with a resolution consistent with the frequency bandwidth involved in the inversion and the aperture illumination provided by the acquisition geometry (Figure 2). Oscillations parallel to the layer in the reconstructed models result from the narrow frequency bandwidth involved in the inversion.

Crosshole test

The crosshole test involves a 4000-m square homogeneous model with 3 anomalies (Figure 3). The model perturbation is composed of 250-m square positive V_P and V_S anomalies, of a 300-m circular negative V_P anomaly and of a 200-m circular negative V_S anomaly respectively. In each case, the amplitude of the V_P and V_S perturbations equals to ± 20 % of the V_P and V_S background velocities respectively. We used isolated V_P and V_S anomalies to assess the coupling between the two parameters during inversion. The crosshole acquisition corresponds to a vertical source line of 71 horizontal forces recorded by a

vertical line of 71 horizontal and vertical sensors (Figure 3). Inversion based on the gradient method was sequentially applied to frequencies 2.9, 4.9, 6.8, 9.8, 12.7 and 16.6 Hz for V_P and V_S parameters. The starting models are the homogeneous V_P and V_S background models. Ten iterations per frequency were computed. The reconstructed V_P and V_S models are shown in Figure 4. Figure 5 shows vertical profiles crossing anomalies at horizontal distances of 1410 m and 2500 m respectively. Heterogeneities are well located, focused and uncoupled: no perturbation are observed in the V_P model at the location of the isolated V_S anomaly and reciprocally. Resolution of the V_S model is higher that of the V_P one due to shorter propagated wavelengths. Limited-bandwidth effects, resulting from to the limited bandwidth of the source and the limited aperture illumination respectively, clearly affect the shape of the reconstructed anomalies and mainly correspond to a deficit of small wavenumbers for the vertical cross-section of the anomalies (Figure 5).

Hill Model test

The hill model is a 1D velocity gradient model below a topography with a Gaussian shape (Figure 6). The model perturbation is composed of a 300-m circular V_P anomaly of amplitude -200 m/s and of a 200-m circular V_S anomaly of amplitude -500 m/s representating two Poisson ratio (ν) anomalies of 0.17 and 0.42 respectively with respect to the background model where $\nu = 0.25$. Eighty-six explosive sources were located 60 m below topography with a 80 m spacing and were recorded by eighty six vertical and horizontal sensors located 30 m below topography. Inversion based on the conjugate gradient algorithm was sequentially applied to frequencies 2.9, 4.9, 6.8, 9.8, 12.7 and 16.6 Hz for V_P and V_S parameters. The starting model is the velocity gradient background. Ten iterations per frequency were computed. Reconstructed models are shown in Figure 7 where both V_P and V_S anomalies can be clearly observed with again a higher resolution for the V_S anomaly. Vertical profiles across the V_P and V_S anomalies allow to assess the quantitative reconstruction of the elastic parameters (Figure 8). One can note a coupling between V_P and V_S parameters at the location of the V_S anomaly where the reconstructed V_P perturbations are not niil. Like in the previous example, we also observed a deficit of small wavenumbers in the shape of the anomalies along the vertical direction due to the surface-to-surface illumination.

CONCLUSION

We have implemented a massively parallel 2D frequency-domain full-waveform inversion algorithm for elastic parameters reconstruction based on a finite volume P_0 forward problem. We validated this algorithm against simple synthetic examples. Future works will both concern improvement of the forward problem algorithm and application of the inverse problem to realistic synthetic case studies. Concerning the forward problem, we will investigate frequency-domain P_1 Discontinuous-Galerkin method which theoretically gives the required accurate solutions of elastic wave propagation in unstructured meshes. We may adapt the mesh to the local propagated wavelength in order to reduce the size of linear systems to be solved. Concerning the inverse problem, applications to realistic synthetic models should be first tackled to better assess the sensitivity of the inversion to the acquisition geometry, to the choice of the elastic parameters and to the surface waves for onshore applications before considering application to real data.

ACKNOWLEDGMENTS

This work is partially funded by the SEISCOPE consortium (http://seiscope.unice.fr), which is sponsored by BP, CGG-VERITAS, EXXON-MOBIL, SHELL and TOTAL, and by the Agence Nationale de la Recherche (ANR) through the project ANR-05-NT05-242427. The LU factorization of the impedance matrix is performed with the MUMPS package. The mesh generation is performed with the help of TRIANGLE software. The access to the high-performance computing facilities of the MESOCENTRE SIGAMM computer center provided the required computer resources, and we gratefully acknowledge both this facility and the support of the staff, and in particular A. Miniussi.

```
# Initialization of Datas ( read mesh files, starting physical parameters file,
acquisition files)
# Loop over group of frequencies [ ifreqgroup for 1 - > Nfreqgroup ]
  # Loop over iterations [ it for 1 -> itermax ]
    # Initialization of Gradient, Preconditionner and cost Function
    # Loop over frequencies in current group [ ifreq for 1 -> nfreq ]
      # Build impedance matrix
      # Parallel Factorization of impedance matrix with MUMPS
      # Preconditionner Computation (if it = 1)
        -> Build RHS table for shots and receivers components ( Vx & Vz )
           positions
        -> Parallel Solve of multi-RHS with MUMPS
        -> Point-to-Point Communications to exchange FPSs of subdomains
           interfaces cells
        -> Computation of preconditionner on local subdomain of each
           processor
        -> Gathering Preconditionner on master processor
      # Gradient Computation
        -> Build RHS table for shots positions
        -> Parallel Solve of multi-RHS with MUMPS
        -> Extract wavefield at receivers positions and send data to master
           processor
        -> Estimate source, computation of residuals and partial cost function
        -> Build RHS table for receivers components positions for
           backpropagating
           of residuals
        -> Parallel Solve of multi-RHS with MUMPS
        -> Point-to-Point Communications to exchange FPSs of subdomains
           interfaces cells
        -> Computation of Gradient on local subdomain of each processor
        -> Gathering Gradient on master processor
    # End Loop
     # Application of Preconditionner to Gradient
     # Compute descent steplength by parabola fitting
     # Compute perturbation and updated model
  # End Loop
# End Loop
```

Figure 1: Parallel implementation of FWI algorithm. Sequential tasks on master processor are in green, parallel ones in red

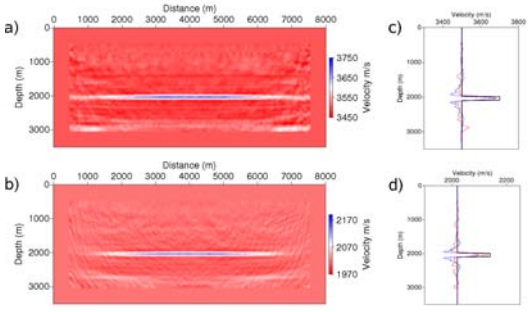

Figure 2: Layer model : Reconstructed models and vertical profile at distance 4000 m for V_P (a,c) and V_S (b,d) parameters.The true, reconstructed and filtered (1.5 to 13.5 Hz) models are plotted with solid black, dash red and dash blue lines respectively

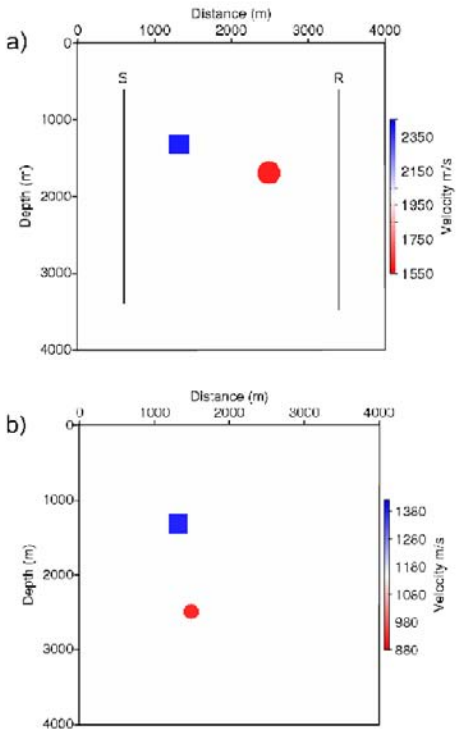

Figure 3: Crosshole test. True V_P (a) and V_S (b) models. S and R denote the source and receiver lines respectively.

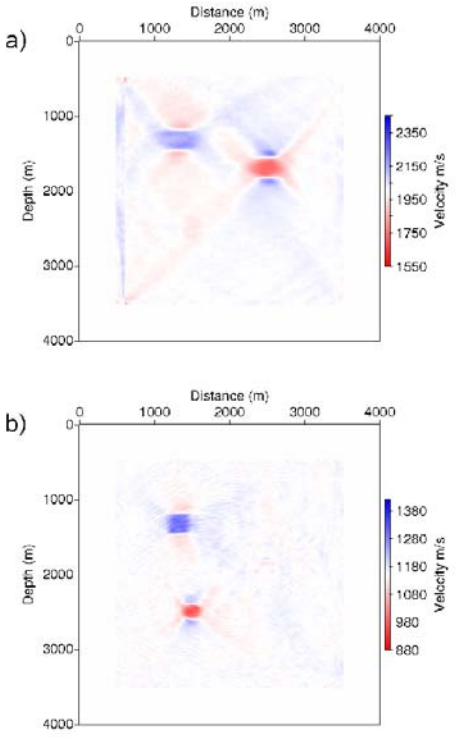

Figure 4: Crosshole test. Reconstructed V_P (a) and V_S (b) models. Note the good uncoupling between V_P and V_S paremeters.

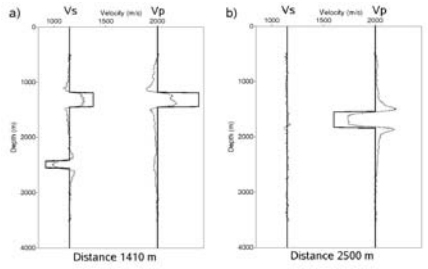

Figure 5: Vertical profiles across anomalies at distances a) 1410 m and b) 2500 m. The true and reconstructed profils are plotted with solid and dash lines respectively.

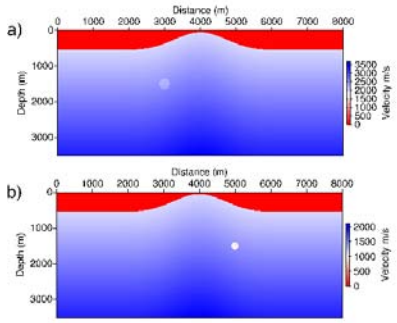

Figure 6: True Hill model. a) V_P model b) V_S model.

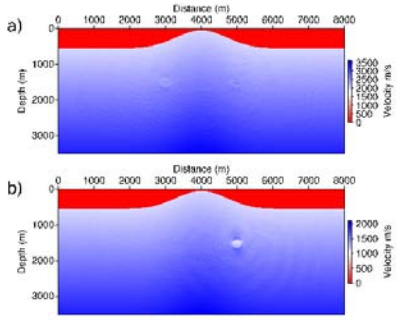

Figure 7: Reconstructed Hill models for a) V_P and b) V_S parameters.

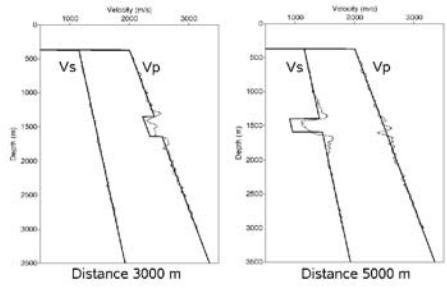

Figure 8: V_P and V_S vertical profiles across the V_P (left) and V_S (right) anomalies. The true and reconstructed profils are plotted with solid and dash lines respectively.

REFERENCES

Amestoy, P. R., A. Guermouche, J. Y. L'Excellent, and S. Pralet, 2006, Hybrid scheduling for the parallel solution of linear systems: Parallel computing, **32**, 136–156.

Berenger, J.-P., 1994, A perfectly matched layer for absorption of electromagnetic waves: Journal of Computational Physics, **114**, 185–200.

Brossier, R., J. Virieux, and S. Operto, 2007, Finite-volume method for 2D PSV elastodynamic equations in frequency domain with velocity-parsimonious formulation: 77^{th} Annual SEG Meeting and Exposition, Expanded Abstracts, 2094–2098, Soc. Expl. Geophys.

Gelis, C., J. Virieux, and G. Grandjean, 2007, 2D elastic waveform inversion using Born and Rytov approximations in the frequency domain: Geophysical Journal International, **168**, 605–633.

Hustedt, B., S. Operto, and J. Virieux, 2004, Mixed-grid and staggered-grid finite difference methods for frequency domain acoustic wave modelling: Geophysical Journal International, **157**, 1269–1296.

Mora, P. R., 1987, Nonlinear two-dimensional elastic inversion of multi-offset seismic data: Geophysics, **52**, 1211–1228.

Operto, S., J. Virieux, J. X. Dessa, and G. Pascal, 2006, Crustal imaging from multifold ocean bottom seismometers data by frequency-domain full-waveform tomography: application to the eastern Nankai trough: Journal of Geophysical Research, **111**, doi:10.1029/2005JB003835.

Pratt, R. G., C. Shin, and G. J. Hicks, 1998, Gauss-Newton and full Newton methods in frequency-space seismic waveform inversion: Geophysical Journal International, **133**, 341–362.

Pratt, R. G., Z. M. Song, and M. Warner, 1996, Two-dimensional velocity models from wide-angle seismic data by wavefield inversion: Geophysical Journal International, **124**, 323–340.

Pratt, R. G. and M. H. Worthington, 1990, Inverse theory applied to multi-source cross-hole tomography. Part 1: acoustic wave-equation method: Geophysical Prospecting, **38**, 287–310.

Ravaut, C., S. Operto, L. Improta, J. Virieux, A. Herrero, and P. dell'Aversana, 2004, Multi-scale imaging of complex structures from multi-fold wide-aperture seismic data by frequency-domain full-wavefield inversions: application to a thrust belt: Geophysical Journal International, **159**, 1032–1056.

Shin, C., K. Yoon, K. J. Marfurt, K. Park, D. Yang, H. Y. Lim, S. Chung, and S. Shin, 2001, Efficient calculation of a partial derivative wavefield using reciprocity for seismic imaging and inversion: Geophysics, **66**, 1856–1863.

Sirgue, L. and R. G. Pratt, 2004, Efficient waveform inversion and imaging : a strategy for selecting temporal frequencies: Geophysics, **69**, 231–248.

Tarantola, A., 1986, A strategy for non linear inversion of seismic reflection data: Geophysics, **51**, 1893–1903.

———, 1987, Inverse problem theory: methods for data fitting and model parameter estimation: Elsevier.